



Hexamolybdenum Clusters Supported on Graphene Oxide: Visible-Light Induced Photocatalytic Reduction of Carbon Dioxide into Methanol

Pawan Kumar, Harshal P. Mungse, Stéphane Cordier, Rabah Boukherroub, Om P. Khatri, Suman L Jain

► To cite this version:

Pawan Kumar, Harshal P. Mungse, Stéphane Cordier, Rabah Boukherroub, Om P. Khatri, et al.. Hexamolybdenum Clusters Supported on Graphene Oxide: Visible-Light Induced Photocatalytic Reduction of Carbon Dioxide into Methanol. Carbon, 2015, 94, pp.91-100. 10.1016/j.carbon.2015.06.029 . hal-01166772

HAL Id: hal-01166772

<https://hal-univ-rennes1.archives-ouvertes.fr/hal-01166772>

Submitted on 19 Nov 2015

HAL is a multi-disciplinary open access archive for the deposit and dissemination of scientific research documents, whether they are published or not. The documents may come from teaching and research institutions in France or abroad, or from public or private research centers.

L'archive ouverte pluridisciplinaire **HAL**, est destinée au dépôt et à la diffusion de documents scientifiques de niveau recherche, publiés ou non, émanant des établissements d'enseignement et de recherche français ou étrangers, des laboratoires publics ou privés.

Hexamolybdenum Clusters Supported on Graphene Oxide: Visible-Light Induced Photocatalytic Reduction of Carbon Dioxide into Methanol

Pawan Kumar,^a Harshal P. Mungse,^a Stéphane Cordier,^b Rabah Boukherroub^c Om P. Khatri,^a and Suman L. Jain^{*a}

^aChemical Sciences Division, CSIR-Indian Institute of Petroleum, Dehradun 248005, India

^bInstitut des Sciences Chimiques de Rennes, UMR 6226 UR1-CNRS, Université de Rennes 1, Campus de Beaulieu, 35042 Rennes Cedex, France

^cInstitut d'Electronique, de Microélectronique et de Nanotechnologie (IEMN), UMR CNRS 8520, Université Lille1, Avenue Poincaré – BP 60069, 59652 Villeneuve d'Ascq, France

Email : sumanjain@iip.res.in

Abstract: Hexamolybdenum (Mo_6) cluster-based compounds namely $\text{Cs}_2\text{Mo}_6\text{Br}_8^{\text{i}}\text{Br}_6^{\text{a}}$ and $(\text{TBA})_2\text{Mo}_6\text{Br}_8^{\text{i}}\text{Br}_6^{\text{a}}$ (TBA = tetrabutylammonium) were immobilized on graphene oxide (GO) nanosheets by taking advantage of the high lability of the apical bromide ions with oxygen-functionalities of GO nanosheets. The loading of Mo_6 clusters on GO nanosheets was probed by Fourier-transform infrared (FTIR) spectroscopy, X-ray photoelectron spectroscopy (XPS), high resolution transmission electron microscopy (HRTEM) and elemental mapping analyses. The developed $\text{GO-Cs}_2\text{Mo}_6\text{Br}_8^{\text{i}}\text{Br}_x^{\text{a}}$ and $\text{GO-(TBA)}_2\text{Mo}_6\text{Br}_8^{\text{i}}\text{Br}_x^{\text{a}}$ composites were then used as heterogeneous photocatalysts for the reduction of CO_2 under visible light irradiation. After 24 h visible light illumination, the yield of methanol was found to be 1644 and 1294 $\mu\text{mol.g}^{-1}\text{cat}$ for $\text{GO-Cs}_2\text{Mo}_6\text{Br}_8^{\text{i}}\text{Br}_x^{\text{a}}$ and $\text{GO-(TBA)}_2\text{Mo}_6\text{Br}_8^{\text{i}}\text{Br}_x^{\text{a}}$, respectively. The quantum yields of methanol by using $\text{GO-Cs}_2\text{Mo}_6\text{Br}_8^{\text{i}}\text{Br}_x^{\text{a}}$ and $\text{GO-(TBA)}_2\text{Mo}_6\text{Br}_8^{\text{i}}\text{Br}_x^{\text{a}}$ as catalysts with reference to Mo_6 cluster units presented in 0.1g amount of catalyst were found to be 0.015 and 0.011, respectively. The role of immobilized Mo_6 clusters-based compounds on GO nanosheets is discussed to understand the photocatalytic mechanism of CO_2 reduction into methanol.

Keywords: Graphene oxide; Mo cluster compound; photocatalysis; carbon dioxide reduction; methanol.

1.0 Introduction

Graphene oxide (GO), an oxidized form of graphene, conventionally served as a most established precursor for the preparation of reduced graphene oxide, chemically functionalized graphene and graphene-based composites [1-2]. Owing to its rich surface chemistry, high specific surface area and various structural defects, GO has attracted large attention not only as a catalytic material, but also as an excellent nanostructured support for heterogenization of various catalysts for efficient chemical transformations [3-4]. The first report on the catalytic activity of GO was revealed by Bielawski et al. in 2010 for the oxidation of various alcohols and the hydration of various alkynes [5]. Then after, the catalytic performance of GO was expanded for various chemical transformations, including oxidation of thiols, sulphides and olefins, aza-Michael addition of amines to activated alkenes, acetalization of aldehydes, ring-opening polymerization of various cyclic lactones and lactams, Friedel-Crafts addition of indoles to α,β -unsaturated ketones, oxidative coupling of amines to imines, oxidative amidation of aromatic aldehydes, etc [6-11]. The catalytic properties of GO have mainly originated from the presence of various oxygen functionalities and unpaired electrons in the GO scaffold and its very high surface area [2-3]. Recently, Riedo et al have demonstrated that GO is a metastable material, whose structure and chemical functionalities evolve at room temperature [12]. Furthermore, an increase of temperature induces gradual reduction of oxygen functionalities in the GO [13]. The ease of GO aging and reduction during catalytic reactions under mild to high temperature raised the issue of recyclability of GO for chemical transformations [14].

Moreover, the high specific surface area, excellent dispersibility in water/ polar solvents, presence of plenty of oxygen containing functional groups and several structural defects in GO scaffold provide ample opportunities to serve as a nano-structured support for heterogenization of catalytically active metal complexes, organic functionalities, and transition metal clusters for efficient chemical transformations [15-19]. In recent years, several methodologies have been established for immobilization of various nano-materials on the GO nanosheets, which include the use of bi-functional linkers, light-induced immobilization, co-reduction of metal salts in the presence of GO, etc [2,20-22]. In most of these approaches, the oxygen functionalities and

structural defects in the GO scaffold function as anchoring sites for the immobilization of various types of nanomaterials.

Molybdenum octahedral (Mo_6) clusters with the general formula $\text{A}_2\text{Mo}_6\text{X}_8^i\text{X}_6^a$ ($\text{A} = \text{Cs}^+$, $n\text{-(C}_4\text{H}_9)_4\text{N}^+$ and $\text{X} = \text{Br}^-$) exhibit photochemical and redox properties due to delocalization of valence electrons on the metal centers [23-25]. The Mo_6 clusters are face-capped by eight inner ligands (Br^i) through Mo-Br^i bonds having covalent dominant character, and are additionally bonded to six apical ligands (Br^a) through Mo-Br^a linkage having strong ionic character. The dissolution of these clusters affords $[\text{Mo}_6\text{Br}_8^i\text{Br}_6^a]^{2-}$ anionic units, where the Mo_6Br_8^i core constitutes a rigid block that can be functionalized by exchange / replacement of Br^a located at the apical position of the cluster. Owing to their remarkable structural and photo-physical properties, $\text{A}_2\text{Mo}_6\text{X}_8^i\text{X}_6^a$ cluster-based compounds provide immense potential for nanoarchitectonic and photocatalytic applications [26]. Recently, Boukherroub et al. have demonstrated that nanocomposites of Mo_6 clusters, gold nanoparticles and GO exhibited very high photocatalytic activity for the degradation of rhodamine B under visible light irradiation. In these photocatalysts, the Mo_6 cluster absorbs the incident photons and initiates the photocatalytic process [24]. The Mo_6 clusters as homogeneous catalyst could also afford photo-reduction of CO_2 into methanol induced by visible light. However, the need of sacrificial donor and non-recyclability of these clusters make the catalytic process expensive [27].

Due to the rising concentration of CO_2 and the depletion of fossil fuel reserves, there is considerable interest in the development of alternative energy sources [28-30]. Conversion of CO_2 into hydrocarbon fuels utilizing the abundant solar energy can provide a viable solution for both problems simultaneously [31-32]. In this regard, a number of heterogeneous catalysts including metal oxides, sulphides, nitrides and oxynitrides have been investigated for CO_2 reduction, albeit lower quantum yields and poor selectivities are the major drawbacks [33-35]. Molecular catalysis, particularly, based on transition metal complexes, such as rhenium(I) bipyridine, ruthenium(II) polypyridine carbonyl, cobalt (II) trisbipyridine, and cobalt (III) macrocycles in combination with a photosensitizer have been considered to be high performance photocatalysts for CO_2 reduction with relatively high quantum yield and high selectivity of products [36-39]. However, the homogeneous nature and non-recycling ability of these catalysts make them impractical from economical as well as environmental viewpoints. This problem can be overcome by anchoring these complexes to photoactive supports, which not

only provides facile recovery of the catalyst, but also photoactive support and complex may work synergistically for better electron transfer to CO_2 [40-41]. In a recent report, we have demonstrated the photocatalytic activity of Mo_6 clusters for the photoreduction of CO_2 using triethylamine as the sacrificial agent [27]. However, non-recycling ability of the photocatalyst and need of sacrificial donor (triethylamine) are the major drawbacks of the developed method. Herein, $\text{Cs}_2\text{Mo}_6\text{Br}_8^{\text{i}}\text{Br}_6^{\text{a}}$ and $(\text{TBA})_2\text{Mo}_6\text{Br}_8^{\text{i}}\text{Br}_6^{\text{a}}$ cluster-based compounds are systematically immobilized on GO nanosheets by taking advantage of labile nature of the apical bromide ions and oxygen-functionalities of GO nanosheets. The developed $\text{GO}-\text{Cs}_2\text{Mo}_6\text{Br}_8^{\text{i}}\text{Br}_6^{\text{a}}$ and $\text{GO}-\text{(TBA)}_2\text{Mo}_6\text{Br}_8^{\text{i}}\text{Br}_6^{\text{a}}$ composites were then used as heterogeneous photocatalysts for the reduction of CO_2 into methanol (Figure 1).

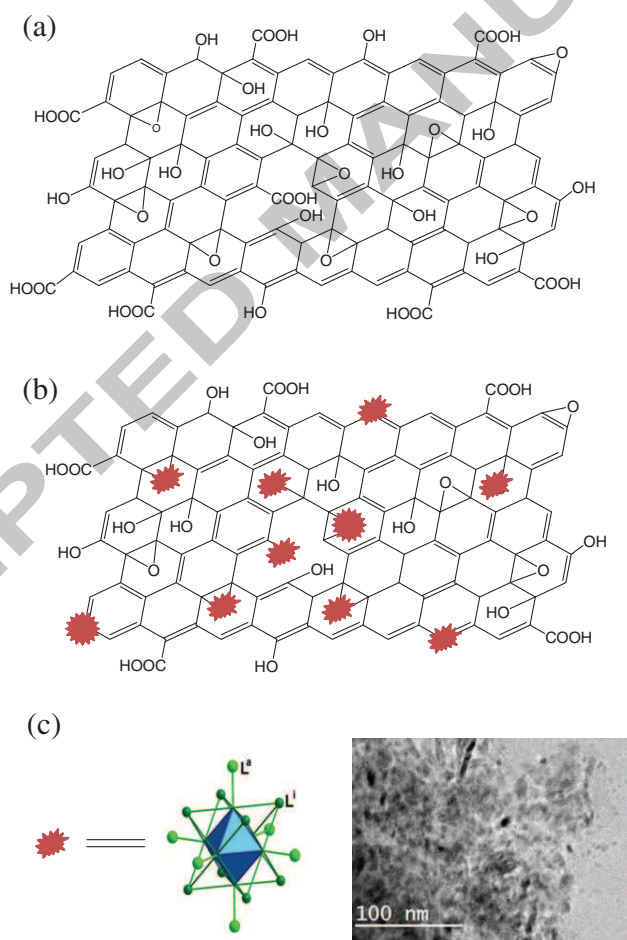


Fig. 1: A schematic illustration of (a) GO nanosheet decorated with various oxygen functionalities, (b) immobilization of $\text{Cs}_2\text{Mo}_6\text{Br}_8^{\text{i}}\text{Br}_6^{\text{a}}$ / $(\text{TBA})_2\text{Mo}_6\text{Br}_8^{\text{i}}\text{Br}_6^{\text{a}}$ clusters on the GO nanosheets, and (c) molecular structure of Mo_6 cluster

representing position of inner and apical ligands and HRTEM image of GO loaded with ample $\text{Cs}_2\text{Mo}_6\text{Br}_8^i\text{Br}_6^a$ / $(\text{TBA})_2\text{Mo}_6\text{Br}_8^i\text{Br}_6^a$ clusters.

2.0 Experimental

2.1 Catalyst preparation

2.1.1 Preparation of $\text{GO}-\text{Cs}_2\text{Mo}_6\text{Br}_8^i\text{Br}_6^a$ / $\text{GO}-(\text{TBA})_2\text{Mo}_6\text{Br}_8^i\text{Br}_6^a$ Composite Materials

The GO, used as a nanostructured support material for immobilization of Mo_6 clusters, was prepared in two steps using graphite powder as a precursor. Initially, graphite powder was oxidized into graphite oxide using a mixture of H_2SO_4 , NaNO_3 and KMnO_4 as strong oxidants and then the oxidized product was washed with H_2O_2 , HNO_3 and ample of water in the subsequent order. In the second step, graphite oxide was exfoliated into GO using ultrasonic probe. The exfoliated product was then centrifuged at 5000 rpm for 15 min to yield two distinct phases: an upper phase containing dispersible fine sheets of GO and a lower deposited semi-solid phase. The fine fraction of GO nanosheets was then used for loading of Mo_6 clusters. The $\text{Cs}_2\text{Mo}_6\text{Br}_8^i\text{Br}_6^a$ / $(\text{TBA})_2\text{Mo}_6\text{Br}_8^i\text{Br}_6^a$ cluster-based compounds were synthesized according to a previously reported procedure [42-43]. In brief, initially, $\text{Mo}_6\text{Br}_{12}$ cluster-based binary bromide was prepared by the reaction of Br_2 with molybdenum powder at 750 °C. Then an excision reaction was performed between a stoichiometric amount of MoBr_2 and CsBr at 850 °C for two days. Afterwards, the prepared $\text{Cs}_2\text{Mo}_6\text{Br}_8^i\text{Br}_6^a$ was dissolved in dry acetone, filtrated and re-crystallized in pure form. $(\text{TBA})_2\text{Mo}_6\text{Br}_8^i\text{Br}_6^a$ was obtained by precipitation after addition of tetrabutyl ammonium bromide in a 50:50 water: ethanol solution of $\text{Cs}_2\text{Mo}_6\text{Br}_8^i\text{Br}_6^a$.

In order to immobilize the synthesized Mo_6 clusters on GO nanosheets, 49 mg of $\text{Cs}_2\text{Mo}_6\text{Br}_8^i\text{Br}_6^a$ or $(\text{TBA})_2\text{Mo}_6\text{Br}_8^i\text{Br}_6^a$ clusters were separately dispersed in a mixture of water and ethanol (100 and 50 mL, respectively). In the subsequent step, a 50 mL of GO aqueous dispersion (2.24 mg/mL) was gradually added into the dispersion of Mo_6 clusters and the mixture was stirred for 48 h at room temperature. This was followed by filtration of the reaction mixture under vacuum line using membrane filter. During this process, the freely suspended $\text{Cs}_2\text{Mo}_6\text{Br}_8^i\text{Br}_6^a$ / $(\text{TBA})_2\text{Mo}_6\text{Br}_8^i\text{Br}_6^a$ clusters passed through the membrane. The filtrate cake, composed of immobilized Mo_6 clusters on GO nanosheets was washed five

times with ethanol to afford the final product, $\text{GO-Cs}_2\text{Mo}_6\text{Br}_8^{\text{i}}\text{Br}_x^{\text{a}}$ or $\text{GO-(TBA)}_2\text{Mo}_6\text{Br}_8^{\text{i}}\text{Br}_x^{\text{a}}$. Finally, the product was dried in an oven for chemical and structural characterizations and then used for photocatalytic reduction of CO_2 . Figure 1 shows the schematic illustrations of GO, Mo_6 clusters and immobilized clusters on the GO nanosheets.

2.2 Chemical and Structural Characterizations of $\text{GO-Cs}_2\text{Mo}_6\text{Br}_8^{\text{i}}\text{Br}_x^{\text{a}}$ / $\text{GO-(TBA)}_2\text{Mo}_6\text{Br}_8^{\text{i}}\text{Br}_x^{\text{a}}$ Composite Materials

Fourier transform infrared (FTIR) spectra of GO, Mo_6 clusters and their composites were recorded on a Thermo-Nicolet 8700 Research spectrophotometer (Thermo Scientific) with a resolution of 4 cm^{-1} . X-ray photoelectron spectroscopy (XPS, JPS-9010TRX, JEOL Ltd.) measurements were carried out using thin films of GO, $\text{GO-Cs}_2\text{Mo}_6\text{Br}_8^{\text{i}}\text{Br}_x^{\text{a}}$ and $\text{GO-(TBA)}_2\text{Mo}_6\text{Br}_8^{\text{i}}\text{Br}_x^{\text{a}}$ samples. The XPS measurements were executed using a $\text{MgK}\alpha$ line as the X-ray source. The peak-fitting of the C1s spectra was performed by using a Gaussian–Lorentzian function after performing a Shirley background correction. Thermogravimetric analyses (TGA) were recorded on a thermal analyzer (Diamond, PerkinElmer). All samples were analyzed in the temperature range of $35\text{--}550\text{ }^\circ\text{C}$ under a steady flow of nitrogen. The high resolution microscopic features of GO, $\text{GO-Cs}_2\text{Mo}_6\text{Br}_8^{\text{i}}\text{Br}_x^{\text{a}}$ and $\text{GO-(TBA)}_2\text{Mo}_6\text{Br}_8^{\text{i}}\text{Br}_x^{\text{a}}$ samples were examined on high resolution transmission electron microscope (HRTEM) by drop casting their ethanol solutions on the TEM grids. Field emission scanning electron microscopy (FESEM) analyses were carried out using an FEI Quanta 200 F. The elemental distribution in the developed composite materials was recorded by using energy dispersive spectrometer (EDS) coupled with FESEM. UV/Vis spectra were measured on a Hitachi U-2900 UV/Vis spectrometer with a path length of 1 cm using quartz cuvettes.

2.3 Photocatalytic Reduction of CO_2

Photocatalytic reduction of CO_2 was carried out using $\text{GO-Cs}_2\text{Mo}_6\text{Br}_8^{\text{i}}\text{Br}_x^{\text{a}}$ and $\text{GO-(TBA)}_2\text{Mo}_6\text{Br}_8^{\text{i}}\text{Br}_x^{\text{a}}$ composites as the photocatalysts. The experiments were performed in borosil cylindrical vessel (100 mL) of 5 cm diameter. Photo-irradiation was carried out under visible light by using 20 W white cold LED flood light (model no. HP-FL-20W-F-Hope LED Opto-Electric Co., Ltd.). The intensity of the light at vessel was measured by intensity meter and was found to be 75 Wm^{-2} . The vessel was charged initially with water (10 mL) and DMF (40 mL), and then the solution was degassed by continuous purging of nitrogen for 15 min.

Subsequently, CO₂ was bubbled through the solution for at least 30 min to saturate the solution, then GO-Cs₂Mo₆Br₈ⁱBr_x^a or GO-(TBA)₂Mo₆Br₈ⁱBr_x^a catalyst (100 mg) was added to the above-described solution. The vessel was tightly closed during the photocatalytic reaction and stirred continuously by a magnetic stirring bar to prevent sedimentation of the catalyst. Samples were collected every 2 h by using a needle, and the catalyst was removed by filtration (0.2 μm PTFE, 13 mm diameter). Quantitative determination of reaction product was achieved by using GC-FID (Varian CP3800 by using CP Sil 24CB LOW BLEED/MS column, flow rate: 0.5 mL.min⁻¹, injector temperature: 250 °C, FID detector temperature: 275 °C). A calibration curve was generated for quantification and for confirmation of linear response of the GC-FID system. Further confirmation of methanol production was done by HPLC (Shimadzu UFLC, by using Oyster BDS Premium C18 250X4.6mm, 5μm column, mobile phase acetonitrile: acetone (65:35), flow rate: 0.5 mL/min at 205 nm). Blank reactions were conducted to ensure that methanol production was due to the photo-reduction of CO₂ and to eliminate surrounding interference. For the determination of gaseous products, 20 μL sample was withdrawn and analyzed with the help of GC-TCD and GC-FID (Agilent 7890A GC system) equipped with RGA (refinery gas analyzer) capillary column; flow rate (H₂: 35 mL/min, air: 350 mL/min, makeup flow: 27 mL/min, for TCD reference flow: 45 mL/min, Helium flow: 2mL/min), injector temperature: 220°C, TCD detector temperature and FID detector temperature: 220°C.

3.0 Results and discussion

3.1 Synthesis and characterization of catalyst

The chemical and structural features of GO and its composites i.e. GO-Cs₂Mo₆Br₈ⁱBr_x^a and GO-(TBA)₂Mo₆Br₈ⁱBr_x^a were thoroughly characterized by FTIR, XPS, TG-DTA, HRTEM, EDX and UV-Vis analyses. The FTIR spectrum of GO (Figure 2) exhibited strong characteristics vibrational bands at 3419, 1732, 1622, 1373, 1263 and 1064 cm⁻¹, which are attributed to O-H stretch, C=O stretch, H₂O bending modes and C=C stretch, O-H bending and C-O stretch, respectively. The strong intensities of these vibrations revealed the presence of ample hydroxyl, epoxy, carboxylic, carbonyl, phenolic, etc. functional groups in the GO scaffold. The Cs₂Mo₆Br₈ⁱBr_x^a has no vibrational signature, except a strong band at 1620 cm⁻¹, attributed to the bending mode of adsorbed water molecules in the cluster compound (Figure 2a).

In contrast, $(\text{TBA})_2\text{Mo}_6\text{Br}_8^{\text{i}}\text{Br}_6^{\text{a}}$ showed strong characteristic vibrational modes in the range of $3000\text{--}2800\text{ cm}^{-1}$, attributed to the C-H stretches of methylene and methyl groups (Figure 2b). Furthermore, strong vibrations at 1466 and 1383 cm^{-1} associated with C-H bending modes revealed the presence of butyl chains in the $(\text{TBA})_2\text{Mo}_6\text{Br}_8^{\text{i}}\text{Br}_6^{\text{a}}$ clusters. The appearance of C-H vibrations in the $\text{GO}-(\text{TBA})_2\text{Mo}_6\text{Br}_8^{\text{i}}\text{Br}_x^{\text{a}}$ composite (inset of Figure 2b) suggested the loading of $(\text{TBA})_2\text{Mo}_6\text{Br}_8^{\text{i}}\text{Br}_6^{\text{a}}$ on the GO nanosheets. Both $\text{GO}-\text{Cs}_2\text{Mo}_6\text{Br}_8^{\text{i}}\text{Br}_x^{\text{a}}$ and $\text{GO}-(\text{TBA})_2\text{Mo}_6\text{Br}_8^{\text{i}}\text{Br}_x^{\text{a}}$ composites exhibited the characteristic vibrations of oxygen functionalities of GO, indicating that most of oxygen functionalities were remained intact and presented in both $\text{GO}-\text{Cs}_2\text{Mo}_6\text{Br}_8^{\text{i}}\text{Br}_x^{\text{a}}$ and $\text{GO}-(\text{TBA})_2\text{Mo}_6\text{Br}_8^{\text{i}}\text{Br}_x^{\text{a}}$ composites. In order to probe the chemical states and plausible interaction between the Mo_6 clusters and GO, all samples were thoroughly characterized by XPS.

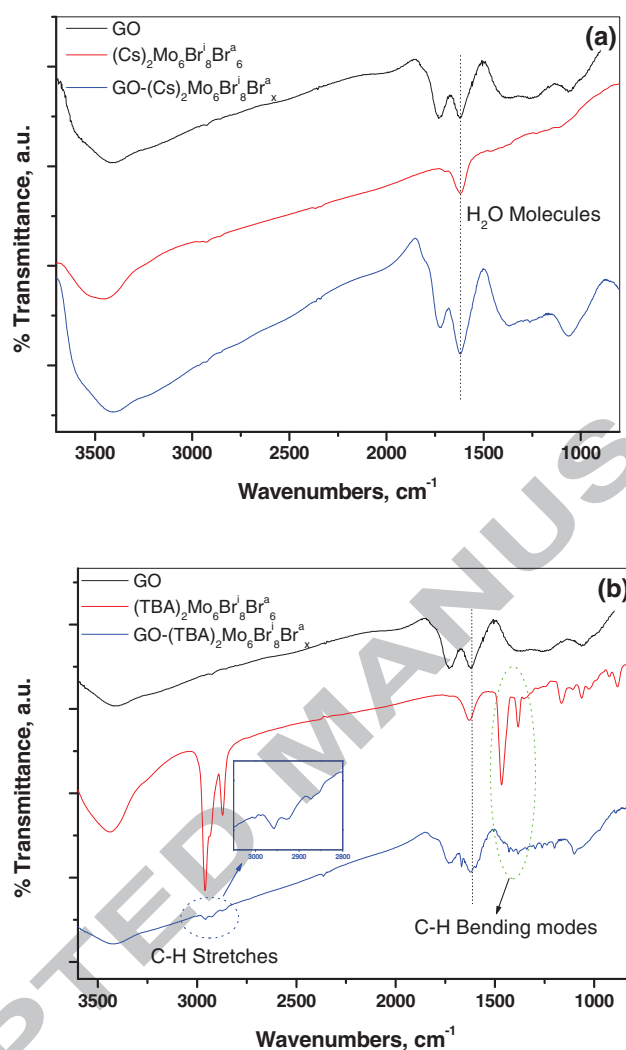


Fig. 2: FTIR spectra of (a) GO, $\text{Cs}_2\text{Mo}_6\text{Br}_8\text{Br}_6^i\text{Br}_6^a$ clusters and $\text{GO-(Cs)}_2\text{Mo}_6\text{Br}_8\text{Br}_6^i\text{Br}_6^a$ composite, and (b) GO, $(\text{TBA})_2\text{Mo}_6\text{Br}_8\text{Br}_6^i\text{Br}_6^a$ clusters and $\text{GO-(TBA)}_2\text{Mo}_6\text{Br}_8\text{Br}_6^i\text{Br}_6^a$ composite. The presence of C-H vibrational modes in $\text{GO-(TBA)}_2\text{Mo}_6\text{Br}_8\text{Br}_6^i\text{Br}_6^a$ composite reveals the loading of $(\text{TBA})_2\text{Mo}_6\text{Br}_8\text{Br}_6^i\text{Br}_6^a$ clusters on the GO nanosheets.

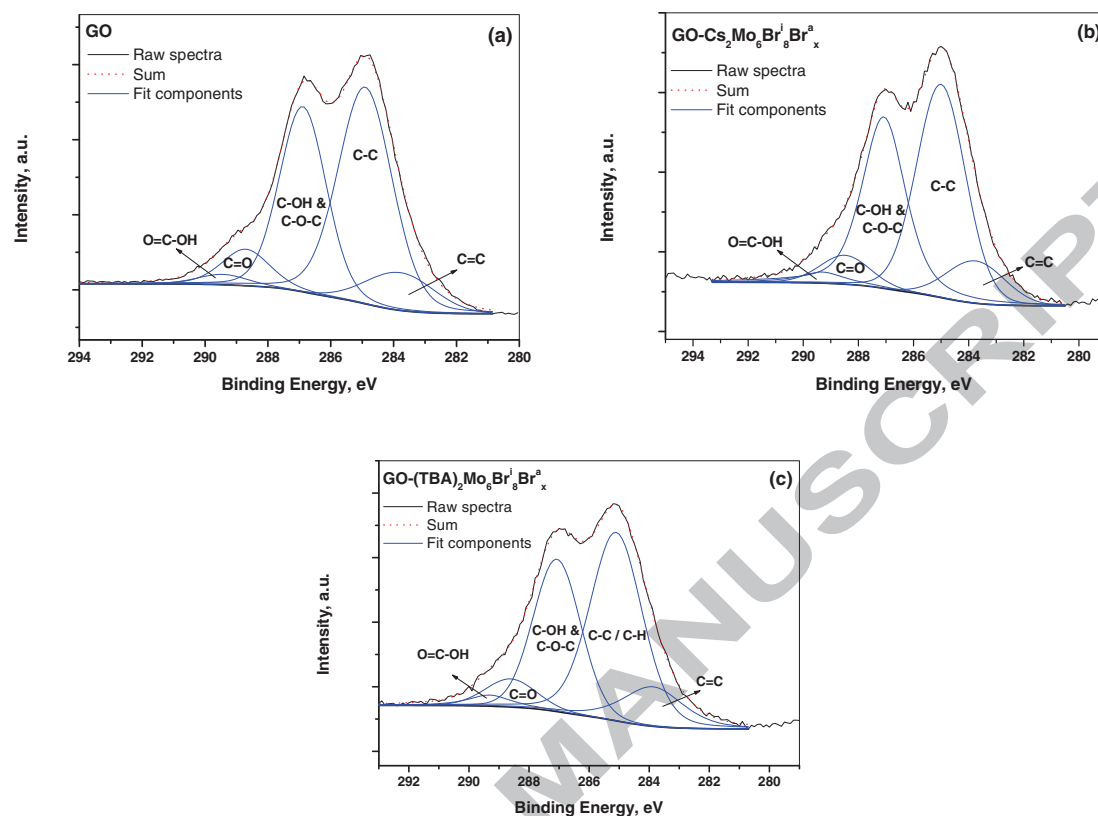
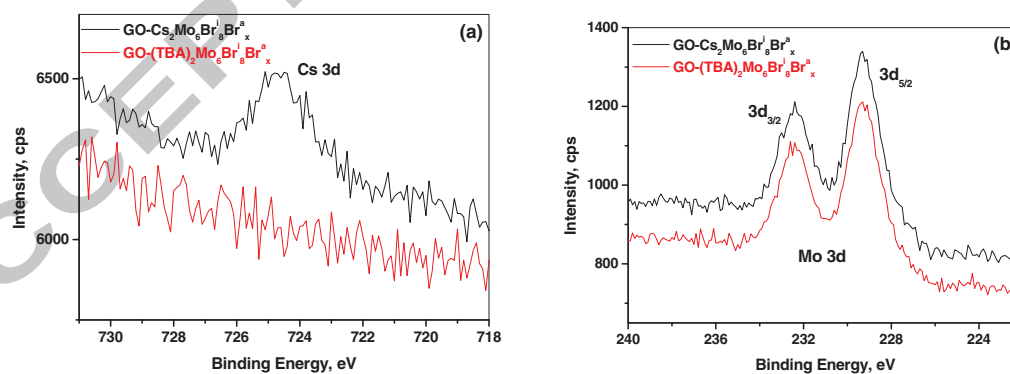


Fig 3: High resolution C1s XPS spectra of (a) GO, (b) GO-Cs₂Mo₆Br₈Br_x and (c) GO-(TBA)₂Mo₆Br₈Br₆ samples. The deconvoluted components illustrate the various types of oxygen functionalities in the materials.



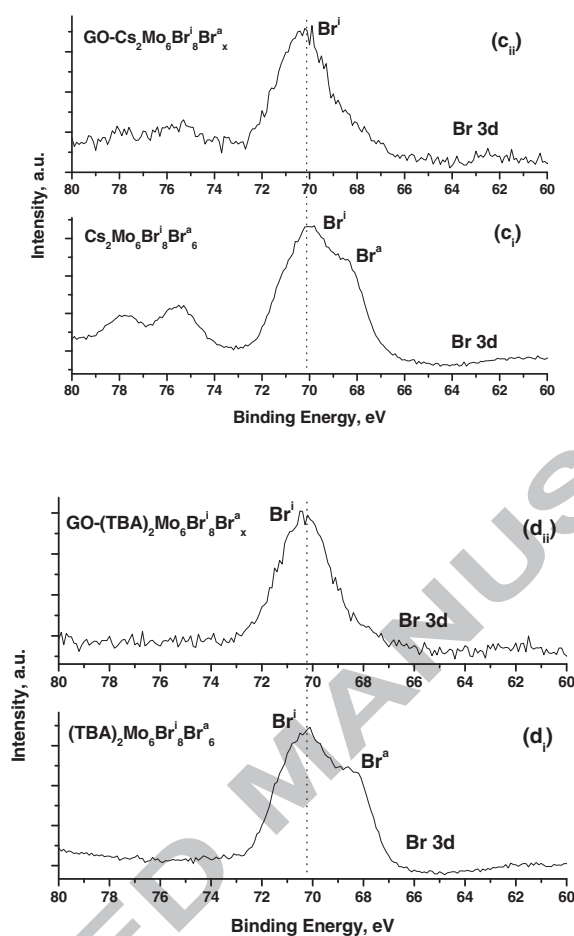


Fig 4: XPS spectra of (a) Cs 3d; (b) Mo 3d; (c) Br 3d regions for $\text{Cs}_2\text{Mo}_6\text{Br}_8\text{Br}_x$ and $\text{GO-Cs}_2\text{Mo}_6\text{Br}_8\text{Br}_x$; (d) Br 3d regions for $(\text{TBA})_2\text{Mo}_6\text{Br}_8\text{Br}_x$ and $\text{GO-(TBA)}_2\text{Mo}_6\text{Br}_8\text{Br}_x$ composites.

XPS analyses of GO, $\text{GO-Cs}_2\text{Mo}_6\text{Br}_8\text{Br}_x$ and $\text{GO-(TBA)}_2\text{Mo}_6\text{Br}_8\text{Br}_x$ samples were carried out to elucidate the quantitative estimation along with chemical changes in the GO and Mo_6 clusters (Figures 3 and 4). The high-resolution C 1s spectrum of GO exhibited an overlapped double peak structure with small tail at higher binding energy attributed to different types of oxygen containing functional groups in the GO scaffold. The peak-fitting of C 1s spectrum of GO can be deconvoluted into five chemically-shifted components (Figure 3a). The C 1s peak centered at 284.9 eV as a major component of GO scaffold is attributed to C-C/C-H carbons. The peak at relatively lower binding energy (284.0 eV) is due to C=C carbon and suggests the presence of

unoxidized domains of sp^2 carbon. Three additional overlapped components at 286.8, 288.6 and 289.5 eV are assigned to the hydroxyl/epoxide (C-OH/C-O-C), carbonyl (C=O) and carboxyl (COOH) functional groups, respectively [44-45]. Figure 3 indicates that all characteristic peaks of C 1s spectra remained intact, when Mo_6 clusters were immobilized on the GO nanosheets and no significant changes were observed. Furthermore, the loading of Mo_6 clusters onto GO nanosheets was deduced by appearance of additional peaks at 724.5, 229.3 and 70.2 eV attributed to Cs 3d, Mo 3d and Br 3d, respectively (Figure 4). The Mo 3d peaks at 229.3 and 232.4 eV are due to the split components of $3d_{5/2}$ and $3d_{3/2}$, respectively and revealed the Mo(II) oxidation state [24,46]. The positions of Mo $3d_{5/2}$ and $3d_{3/2}$ components in the $GO-Cs_2Mo_6Br_8^iBr_x^a$ and $GO-(TBA)_2Mo_6Br_8^iBr_x^a$ are comparable to those obtained for their pure Mo_6 clusters. These results suggest that the cluster core $Mo_6Br_8^i$ remained intact during cluster immobilization on the GO nanosheets. The Cs 3d peaks at 724.5 and 739 eV are attributed to the split components of $3d_{5/2}$ and $3d_{3/2}$, respectively and indicate the presence of Cs(I) in the $GO-Cs_2Mo_6Br_8^iBr_x^a$ composite (Figure 4a). The Cs $3d_{3/2}$ peak couldn't appear explicitly, as it was diminished by nearby strong peak of O (KVV) as shown in Figure S1 (Electronic supporting information).

The internal core of the octahedral Mo_6 clusters consists of eight Mo- Br^i bonds and the remaining six Br^- are placed on apical position through Mo- Br^a bonds having strong ionic character. These apical Br^- functionalities are prone to interact with other chemical functionalities and facilitate their immobilization onto solid supports. The XPS spectra of Mo_6 cluster compounds and their immobilized composites $GO-Cs_2Mo_6Br_8^iBr_x^a$ and $GO-(TBA)_2Mo_6Br_8^iBr_x^a$ are shown in Figure 4c-d. The Br 3d peak in Mo_6 clusters is composed of two components at 70.2 and 68.6 eV, which are attributed to covalently bonded inner Br atoms (Br^i) and apical bromide ions (Br^a) of Mo_6 clusters, respectively [47-48]. The Br 3d spectra of $GO-Cs_2Mo_6Br_8^iBr_x^a$ and $GO-(TBA)_2Mo_6Br_8^iBr_x^a$ composites (Figure 4c-d) showed that the peak component at 68.6 eV, attributed to Br^a ligands, is almost diminished, demonstrating the elimination of Br^a ligands. This suggests the reaction of Br^a of Mo_6 clusters with hydroxyl / oxygen carrying functional groups of GO nanosheets. As a result, Mo_6 clusters immobilized on the GO nanosheets by covalent linkage and Br^a are eliminated during immobilization process. The atomic % of Mo and Br components in both $(TBA)_2Mo_6Br_8^iBr_6^a$ cluster and $GO-(TBA)_2Mo_6Br_8^iBr_x^a$ composites were calculated based on XPS study, to determine the interaction between the $(TBA)_2Mo_6Br_8^iBr_6^a$

cluster and GO nanosheets. The experimental ratio of $\text{Br}/\text{Mo} = 2.6$ in $(\text{TBA})_2\text{Mo}_6\text{Br}_8^i\text{Br}_6^a$ cluster agrees with the theoretical value (2.33). After immobilization of $(\text{TBA})_2\text{Mo}_6\text{Br}_8^i\text{Br}_6^a$ cluster, the ratio of Br/Mo decreased to 1.6, which is closer to the expected value (1.33) for a Br^i/Mo cluster core. Recently, Sutherland et al. have further demonstrated that labile terminal nitro groups at apical position in Mo_6 clusters were eliminated during their chemical attachment to solid supports [49].

UV/Vis absorption spectra of $\text{Cs}_2\text{Mo}_6\text{Br}_8^i\text{Br}_6^a$ and $(\text{TBA})_2\text{Mo}_6\text{Br}_8^i\text{Br}_6^a$ in acetonitrile exhibited sharp peaks at 242 and 243 nm due to the inter ligand transition and small humps at 386 nm and 380 nm due to the metal-to-ligand charge-transfer (MLCT) transitions, respectively (Figure S2a,b). For GO, a characteristic absorption band at 227 nm due to $\pi \rightarrow \pi^*$ transition of discrete units of sp^2 carbon conjugated network and a small hump at 300 nm due to $n \rightarrow \pi^*$ of carbonyl groups were observed. Immobilization of Mo_6 clusters to GO enhanced the overall absorption pattern as shown in Figure S2.

In order to confirm the visible light absorption, we calculated the band gap of GO, $\text{Cs}_2\text{Mo}_6\text{Br}_8^i\text{Br}_6^a$ cluster, GO- $\text{Cs}_2\text{Mo}_6\text{Br}_8^i\text{Br}_x^a$ composite, $(\text{TBA})_2\text{Mo}_6\text{Br}_8^i\text{Br}_6^a$ cluster and GO- $(\text{TBA})_2\text{Mo}_6\text{Br}_8^i\text{Br}_x^a$ composite with the help of Tauc plot as shown in Figure S3. The band gap value for GO was found to be 2.90 eV was in well agreement with the reported literature [50]. For $\text{Cs}_2\text{Mo}_6\text{Br}_8^i\text{Br}_6^a$ and $(\text{TBA})_2\text{Mo}_6\text{Br}_8^i\text{Br}_6^a$ clusters compounds, two band gap values were obtained; the 4.07 eV and 4.16 eV were due to the interligand transitions while the 2.40 eV and 2.47 eV were ascribed to the MLCT transitions, respectively. After immobilization of Mo_6 clusters on GO, the band gap values significantly decreased to 0.9 and 1.5 eV for GO- $\text{Cs}_2\text{Mo}_6\text{Br}_8^i\text{Br}_x^a$ and GO- $(\text{TBA})_2\text{Mo}_6\text{Br}_8^i\text{Br}_x^a$ composite, respectively.

The thermal behaviour of GO, Mo_6 clusters and their composites were examined by thermogravimetric analysis (TGA). GO showed two characteristic major weight losses in the range of 50–110 °C and 170–240 °C, owing to evaporation of trapped water molecules and thermal decomposition of labile oxygen functionalities in GO scaffold, respectively (Figure 5). The $\text{Cs}_2\text{Mo}_6\text{Br}_8^i\text{Br}_6^a$ cluster is found to be thermally stable upto 500 °C, whereas $(\text{TBA})_2\text{Mo}_6\text{Br}_8^i\text{Br}_6^a$ cluster has significant mass loss about 27 % in the range of 320–390 °C with maximum loss at 368 °C, most likely due to the thermal decomposition of TBA units (Figure b_{ii}). However, GO- $(\text{TBA})_2\text{Mo}_6\text{Br}_8^i\text{Br}_x^a$ composite showed 4.5 % weight loss (due to TBA units and oxygen functionalities of GO) in the range of 295–375 °C with maximum loss at 340 °C (Figure b_{iii}). Plausibly, the presence of residual

oxygen functionalities in the $\text{GO-(TBA)}_2\text{Mo}_6\text{Br}_8^{\text{i}}\text{Br}_x^{\text{a}}$ composite has facilitated the decomposition of TBA units in supported composite comparatively at lower temperature. Based on the TGA results, the calculated weight loss due to the supported TBA cluster units was found to be 1.6 %.

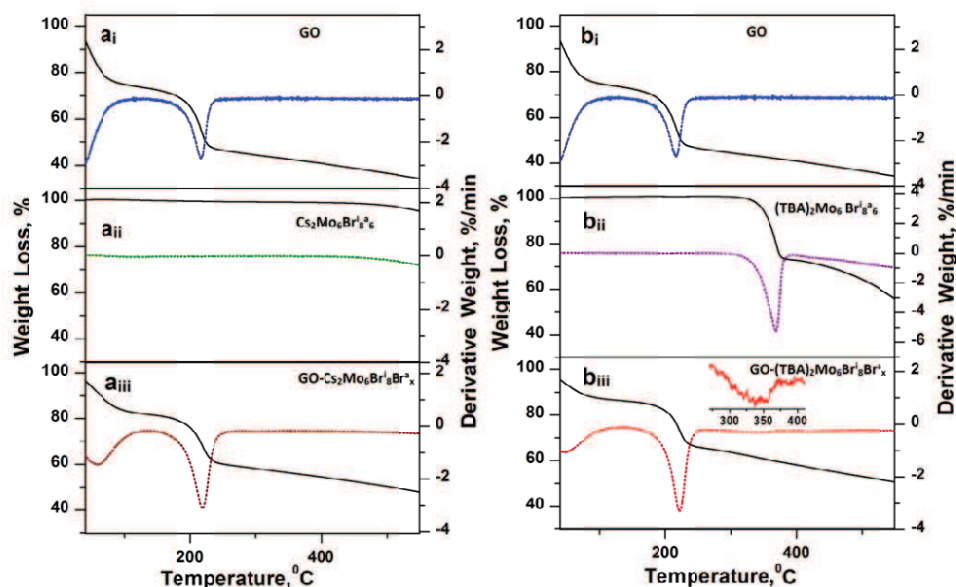


Fig 5: TG-DTA patterns of (a) GO, $\text{Cs}_2\text{Mo}_6\text{Br}_8\text{Br}_6^{\text{i}}$ cluster and $\text{GO-Cs}_2\text{Mo}_6\text{Br}_8\text{Br}_x^{\text{a}}$ composite; (b) GO, $(\text{TBA})_2\text{Mo}_6\text{Br}_8\text{Br}_6^{\text{i}}$ cluster and $\text{GO-(TBA)}_2\text{Mo}_6\text{Br}_8\text{Br}_x^{\text{a}}$ composite over the temperature range of 30-550 °C under nitrogen flow.

The nano-structural features of GO and its composites with Mo_6 clusters were examined by HRTEM. Figure 6a shows plenty of wrinkle and folded regions in the HRTEM image of GO scaffolds. These features are attributed to the sp^3 carbons, which are linked to oxygen functionalities in the basal plane and various structural defects. Significant structural changes are observed when Mo_6 clusters were immobilized on GO nanosheets (Figure 6b-c). The Mo_6 clusters are uniformly distributed over the GO surface and they are seen as dark grey features in the range of 2-10 nm. The hydrodynamic diameter of $\text{Cs}_2\text{Mo}_6\text{Br}_8\text{Br}_6^{\text{i}}$ clusters is reported to be 2.5 nm by dynamic light scattering (DLS) method, whereas the crystallographic cluster unit size of these clusters is 1.1 nm [25]. The larger size of immobilized Mo_6 clusters on GO nanosheets along with their undefined structure suggest that the Mo_6 clusters are immobilized on the GO not only as single unit of each cluster, but also in form of aggregates composed of 2-7 units. Usually, these Mo_6 clusters agglomerate because

of the electrostatic attraction between anionic parts of one cluster unit and counter cationic part of another unit. Furthermore, elemental mapping of $\text{GO-Cs}_2\text{Mo}_6\text{Br}_8\text{Br}_x^{\text{a}}$ and $\text{GO-(TBA)}_2\text{Mo}_6\text{Br}_8\text{Br}_x^{\text{a}}$ composites based on EDS measurements was carried out to reveal the distribution of Mo_6 clusters on the GO nanosheets. Figure S4 (supporting information) shows FESEM micrographs and the corresponding elemental mapping of $\text{GO-Cs}_2\text{Mo}_6\text{Br}_8\text{Br}_x^{\text{a}}$ and $\text{GO-(TBA)}_2\text{Mo}_6\text{Br}_8\text{Br}_x^{\text{a}}$ composites. The through and uniform distribution of cesium, molybdenum and bromide as characteristic elements in $\text{GO-Cs}_2\text{Mo}_6\text{Br}_8\text{Br}_x^{\text{a}}$ composite and nitrogen, molybdenum and bromide in $\text{GO-(TBA)}_2\text{Mo}_6\text{Br}_8\text{Br}_x^{\text{a}}$ composite indicate that Mo_6 clusters are uniformly immobilized on GO nanosheets, which is very important for efficient photocatalytic activities of developed composite materials. The molybdenum content in the $\text{GO-Cs}_2\text{Mo}_6\text{Br}_8\text{Br}_x^{\text{a}}$ and $\text{GO-(TBA)}_2\text{Mo}_6\text{Br}_8\text{Br}_x^{\text{a}}$ composites was found to be 0.74 and 0.73 atomic %, respectively, as determined by XPS analysis.

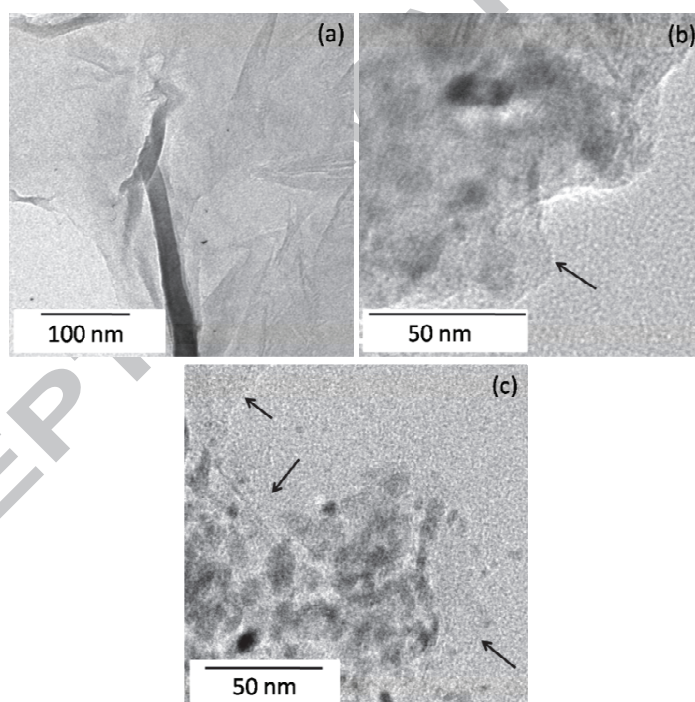


Fig. 6. HRTEM images of (a) GO nanosheets. Distribution of hexamolybdenum clusters on GO nanosheets: (b) $\text{GO-Cs}_2\text{Mo}_6\text{Br}_8\text{Br}_x^{\text{a}}$ and (c) $\text{GO-(TBA)}_2\text{Mo}_6\text{Br}_8\text{Br}_x^{\text{a}}$ composites.

3.2 Photocatalytic reduction of CO_2

The photocatalytic activity of the synthesized $\text{GO-Cs}_2\text{Mo}_6\text{Br}_8\text{Br}_x^{\text{a}}$ and $\text{GO-(TBA)}_2\text{Mo}_6\text{Br}_8\text{Br}_x^{\text{a}}$ composite

materials for CO₂ reduction was examined in water/DMF mixture under visible light irradiation by using 20 watt white cold LED flood light. During the photoreduction, 0.5 mL reaction mixture was withdrawn gradually. Then 1 µL withdrawn reaction mixture was injected in a GC-FID system for quantitative estimation. The performance of the catalysts was evaluated in term of methanol (MeOH) yield as it was the only liquid reduction product. The MeOH yield (µmol.g⁻¹ cat.) with respect to time using Cs₂Mo₆Br₈Br^a₆, (TBA)₂Mo₆Br₈Br^a₆, GO-Cs₂Mo₆Br₈Br^a_x and GO-(TBA)₂Mo₆Br₈Br^a_x composite as catalyst is displayed in Figure 7. Both GO-Cs₂Mo₆Br₈Br^a_x and GO-(TBA)₂Mo₆Br₈Br^a_x exhibited higher photocatalytic activity as compared to GO and Mo₆ clusters. Furthermore, among the two catalysts studied, GO-Cs₂Mo₆Br₈Br^a_x was found to be superior than GO-(TBA)₂Mo₆Br₈Br^a_x. After 24 h illumination, the yield of methanol using GO-Cs₂Mo₆Br₈Br^a_x, GO-(TBA)₂Mo₆Br₈Br^a_x, GO, Cs₂Mo₆Br₈Br^a₆, and (TBA)₂Mo₆Br₈Br^a₆ as catalysts under identical experimental conditions was found to be 1644, 1294, 439, 285 and 238, µmol.g⁻¹cat, respectively with the corresponding methanol formation rate (R_{MeOH}) of 68.5, 53.9, 18.2, 11.8 and 9.9 µmol.g⁻¹cat.h⁻¹, respectively. The turnover number (TON) and quantum yield for Cs₂Mo₆Br₈Br^a₆ cluster were found to be 3.30 and 0.0026, respectively, whereas, for (TBA)₂Mo₆Br₈Br^a₆ cluster the values were 2.75 and 0.0021, respectively. The TON by using GO-Cs₂Mo₆Br₈Br^a_x and GO-(TBA)₂Mo₆Br₈Br^a_x was found to be 19.0, and 10.38 respectively with respect to Mo₆ cluster and the quantum yields of methanol with reference to Mo₆ cluster units presented in 0.1g amount of catalyst were found to be 0.015 and 0.011, respectively. The TON of methanol per mole of graphene oxide was calculated by considering the equivalent formula of GO as C₆(O), which was found to be 0.04. The formation of methanol was further confirmed by HPLC analysis as depicted in Figures S5 and S6. For the quantitative estimation of methanol, a calibration curve was plotted by injecting an exact amount of methanol (1 µL) in GC-FID (Figure S8). Then the concentration of methanol produced by photo-induced CO₂ reduction was calculated by injecting 1.0 µL of the final reaction solution in GC-FID and comparing the peak area with calibration curve for methanol standard. Further HPLC analysis was performed to confirm the formation of methanol as the only liquid product obtained from the photoreduction of CO₂. Gaseous reaction products were analyzed by GC-FID and GC-TCD and confirmed that there was no gaseous product such as H₂, CO, CH₄ formed during the photoreduction of CO₂. As methanol was obtained as the only product from CO₂ photoreduction under the described experimental conditions, so the catalytic selectivity (CS)

of GO-Mo₆ clusters was 100 %.

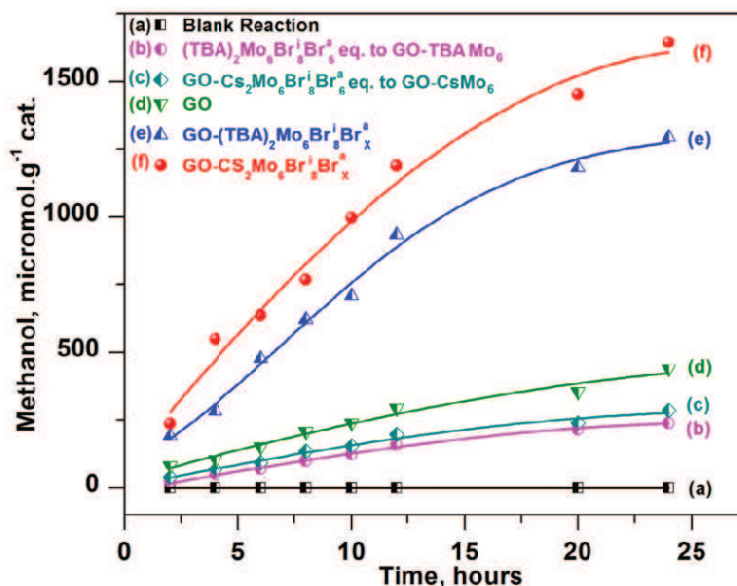


Fig 7: Methanol formation rate in (a) blank reaction, (b, c) using (TBA)₂Mo₆Br₈Br₆^a and Cs₂Mo₆Br₈Br₆^a in equimolar amounts as presented in GO-composites, (d) GO, (e) GO-(TBA)₂Mo₆Br₈Br₆^a and (f) GO-Cs₂Mo₆Br₈Br₆^a catalyzed photoreduction of CO₂.

Blank experiments were conducted to ensure that the product formed was due to CO₂ photoreduction. The blank tests consisted of visible light irradiation in the absence of catalyst (Table 1, entry 1) and reaction in the dark with the catalyst (Table 1, entry 2) under otherwise identical experimental conditions. An additional blank test was performed by illuminating the reaction mixture in the presence of photocatalyst by filling N₂ rather than CO₂ (Table 1, entry 3). In all cases, no organic product was obtained even after 24 h visible light exposure.

Table: 1 Photocatalytic reduction of CO₂ into methanol under controlled experimental conditions

Entry	Catalyst	React. Precursor	Visible Light Illumination	T/ h	TON
1	Nil	CO ₂	Yes	24	-
2	GO- Cs ₂ Mo ₆ Br ₈ ^j Br _x ^a	CO ₂	No	24	-
3	GO- Cs ₂ Mo ₆ Br ₈ ^j Br _x ^a	N ₂	Yes	24	-
4	Cs ₂ Mo ₆ Br ₈ ^j Br ₆ ^a	CO ₂	Yes	24	3.30
5	(TBA) ₂ Mo ₆ Br ₈ ^j Br ₆ ^a	CO ₂	Yes	24	2.75
4	GO	CO ₂	Yes	24	0.04
5	GO- Cs ₂ Mo ₆ Br ₈ ^j Br _x ^a	CO ₂	Yes	24	19.0
6	GO- (TBA) ₂ Mo ₆ Br ₈ ^j Br _x ^a	CO ₂	Yes	24	10.38

Last but not least, we established the recycling of the developed heterogeneous cluster catalysts. The results of these recycling experiments are exhibited in Figure 8. As shown, both heterogeneous GO-Mo photocatalysts exhibited efficient recycling for four runs and provided almost similar yield of methanol under identical experimental conditions. These studies suggested that the developed catalysts were highly stable and the reaction was truly heterogeneous in nature.

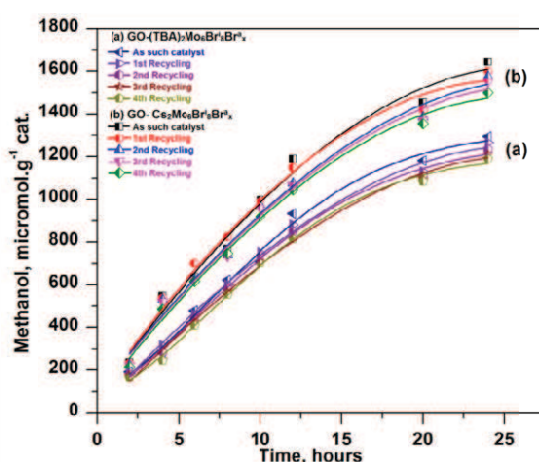


Fig: 8 Recycling experiments using (a) GO- (TBA)₂Mo₆Br₈^jBr_x^a and (b) GO- Cs₂Mo₆Br₈^jBr_x^a.

A plausible mechanism for the CO₂ photoreduction to methanol using GO immobilized Mo₆ clusters as catalysts on the basis of their band gap is illustrated in Figure 9. The presence of oxygen containing functionalities on GO transforms aromatic sp² carbons into sp³ carbons and creates a network of enormous sp² (conduction band) and sp³ carbon domains (valence band) on GO sheet. Due to presence of several conductive sp² carbon domains and non conductive sp³ carbon containing domains on GO sheet, a band gap is created and it works like a semiconductor [51-53]. The band gap for GO was found to be 2.9 eV in good agreement with the literature values of 2.9-3.7 eV as reported by Hsu et al. [50]. On the other hand, Mo₆ clusters due to their lower band gap values have good visible light absorbance; hence to improve the performance of GO in visible light, Mo₆ clusters were immobilized on the surface of GO *via* replacement of labile bromine atoms. After absorption of visible light, Mo₆ cluster was transformed to excited state Mo₆* by HOMO to LUMO transition and the excited Mo₆* transfers electron to the conduction band of GO (Fig. 9). These electrons in the conduction band of GO were used for the reduction of CO₂ to give methanol [54-56]. The positively charged Mo₆⁺ cluster gets electron from valence band of GO and transforms back into its original (Mo₆) state. Water splitting at the valence band of GO possibly provides necessary electrons and protons for the reduction of CO₂ to methanol. Furthermore, due to the better charge mobility and higher surface area, GO improves the catalytic performance synergistically [57-59].



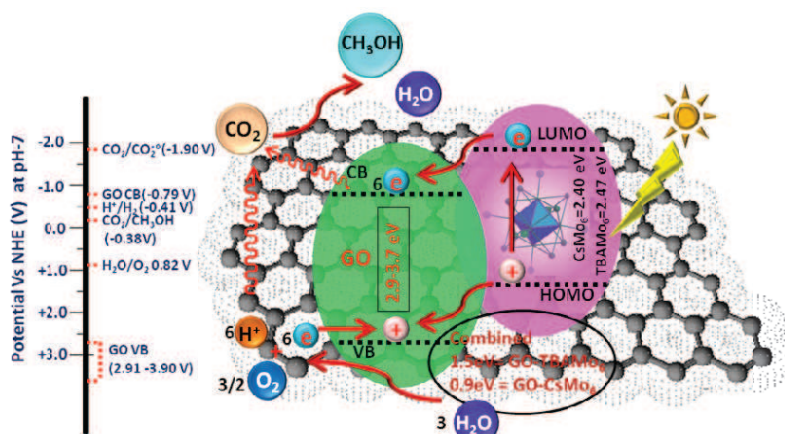


Fig. 9 Plausible mechanism of photoreduction of CO₂ into methanol catalyzed by GO-hexamolybdenum composite

4.0 Conclusion

Hexamolybdenum cluster compounds i.e. Cs₂Mo₆Br₈Br_x^a and (TBA)₂Mo₆Br₈Br_x^a were immobilized on GO nanosheets and the resulting composites were used for the photocatalytic reduction of CO₂ to methanol under visible light irradiation without adding any sacrificial agent. Owing to the wide band gap, GO alone does not provide excitation in the visible. The Mo₆ units located on the surface of GO act as visible light absorbers and facilitate the transfer of electrons to GO conduction band. After 24 h of visible light illumination, the yield of methanol was found to be 1644 and 1294 μmol.g⁻¹cat for GO-Cs₂Mo₆Br₈Br_x^a and GO(TBA)₂Mo₆Br₈Br_x^a, respectively. These values are much higher than GO alone (439 μmol.g⁻¹cat). However, the facile recovery, efficient recycling and no need of sacrificial donors such as triethylamine make the developed methodology superior and more advantageous for converting CO₂ to high value chemicals.

Acknowledgement

We kindly acknowledge Director, CSIR-IIP for his permission to publish these results. PK and HPM are thankful to CSIR and UGC, New Delhi, respectively for providing research fellowship. Analytical department of the Institute is kindly acknowledged for providing support in analysis. DST, New Delhi is kindly acknowledged for providing financial support.

Notes and references

- [1] D. R. Dreyer, S. Park, C. W. Bielawski and R. S. Ruoff, *Chem. Soc. Rev.* 39 (2010) 228-240.
- [2] V. Georgakilas, M. Otyepka, A. B. Bourlinos, V. Chandra, N. Kim, K. C. Kemp, P. Hobza, R. Zboril and K. S. Kim, *Chem. Rev.* 112 (2012) 6156-6214.
- [3] S. Navalon, A. Dhakshinamoorthy, M. Alvaro and H. Garcia, *Chem. Rev.* 114 (2014) 6179-6212.
- [4] D. R. Dreyer, A. D. Todd and C. W. Bielawski, *Chem. Soc. Rev.* 43 (2014) 5288-5301.
- [5] D. R. Dreyer, H. P. Jia and C. W. Bielawski, *Angew. Chem. Int. Ed.* 49 (2010) 6813-6816.
- [6] H. P. Jia, D. R. Dreyer and C. W. Bielawski, *Adv. Synth. Catal.* 353 (2011) 528-532.
- [7] D. R. Dreyer, H. P. Jia, A. D. Todd, J. Geng and C. W. Bielawski, *Org. Biomol. Chem.* 9 (2011) 7292-7295.
- [8] S. Verma, H. P. Mungse, N. Kumar, S. Choudhary, S. L. Jain, B. Sain and O. P. Khatri, *Chem. Commun.* 47 (2011) 12673-12675.
- [9] A. Dhakshinamoorthy, M. Alvaro, M. Puche, V. Fornes, and H. Garcia, *Chem. Cat. Chem.* 4 (2012) 2026-2030.
- [10] D. R. Dreyer, K. A. Jarvis, J. P. Ferreira and C. W. Bielawski, *Polym. Chem.* 3 (2012) 757-766.
- [11] C. Su, M. Acik, K. Takai, J. Lu, S. Hao, Y. Zheng, P. Wu, Q. Bao, T. Enoki, Y. J. Chabal and K. P. Loh, *Nat. Commun.* 3 (2012) 1298.
- [12] S. Kim, S. Zhou, Y. Hu, M. Acik, Y. J. Chabal, C. Berger, W. Heer, A. Bongiorno and E. Riedo, *Nat. Mater.* 11 (2012) 544-549.
- [13] S. Choudhary, H. P. Mungse and O. P. Khatri, *Chem. Asian J.* 8 (2013) 2070-2078.
- [14] H. P. Mungse, N. Bhakuni, D. Tripathi, O. P. Sharma, B. Sain and O. P. Khatri, *J. Phys. Org. Chem.* 27 (2014) 944-951.
- [15] Y. Li, W. Gao, L. Ci, C. Wang and P. M. Ajayan, *Carbon* 48 (2010) 1124-1130.
- [16] G. M. Scheuermann, L. Rumi, P. Steurer, W. Bannwarth and R. Mulhaupt, *J. Am. Chem. Soc.* 131 (2009) 8262-8270.
- [17] J. Huang, L. Zhang, B. Chen, N. Ji, F. Chen, Y. Zhang and Z. Zhang, *Nanoscale* 2 (2010) 2733-2738.

- [18] H. P. Mungse, S. Verma, N. Kumar, B. Sain and O. P. Khatri, *J. Mater. Chem.* 22 (2012) 5427–5433.
- [19] C. Yuan, W. Chen and L. Yan, *J. Mater. Chem.*, 22 (2012) 7456–7460.
- [20] P. V. Kamat, *J. Phys. Chem. Lett.* 1 (2010) 520-527.
- [21] G. Moon, H. Kim, Y. Shin and W. Choi, *RSC Adv.* 2 (2012) 2205-2207.
- [22] G. Williams and P. V. Kamat, *Langmuir* 25 (2009) 13869-13873.
- [23] A. W. Maverick, J. S. Najdzonek, D. Mackenzie, D. G. Nocera and H. B. Gray, *J. Am. Chem. Soc.* 105 (1983) 1878-1882.
- [24] A. Barras, M. R. Das, R. R. Devarapalli, M. V. Shelke, S. Cordier, S. Szunerits and R. Boukherroub, *Appl. Catal. B* 130-131 (2013) 270-276.
- [25] F. Grasset, F. Dorson, S. Cordier, Y. Molard, C. Perrin, A. M. Marie, T. Sasaki, H. Haneda, Y. Bando and M. Mortier, *Adv. Mater.* 20 (2008) 143-148.
- [26] S. Cordier, F. Grasset, Y. Molard, M. Amela-Cortes, R. Boukherroub, S. Ravaine, M. Mortier, N. Ohashi, N. Saito and H. Haneda, *J. Inorg. Organomet. Polym. Mater.* 25 (2015) 189–204.
- [27] P. Kumar, S. Kumar, S. Cordier, S. Paofai, R. Boukherroub and S. L. Jain, *RSC Adv.* 4 (2014) 10420-10423.
- [28] G. A. Olah, *Angew. Chem. Int. Ed.* 52 (2013) 104–107.
- [29] M. Aresta, Carbon dioxide reduction and use as a chemical feedstock, Tolman, W.B., Ed.; Wiley-VCH: Weinheim, Germany, 2006, 1–41.
- [30] V. P. Indrakanti, J. D. Kubicki, and H. H. Schobert, *Energy Environ. Sci.* 2 (2009) 745–758.
- [31] P. D. Tran, L. H. Wong, J. Barber and J. S. C. Loo, *Energy Environ. Sci.* 5 (2012) 5902.
- [32] Halmann M. M.; Steinberg M. *Greenhouse Gas Carbon Dioxide Mitigation Science and Technology*, Lewis Publishers, Boca Raton, Florida. 1999.
- [33] Y. Izumi, *Coord. Chem. Rev.* 257 (2013) 171-186.
- [34] S. N. Habisreutinger, L. S. Mende, and J. K. Stolarczyk, *Angew. Chem. Int. Ed.* 52 (2013) 7372-7408.
- [35] A. J. Cowan and J. R. Durrant, *Chem. Soc. Rev.* 42 (2013) 2281-2293.
- [36] A. J. Morris, G. J. Meyer and E. Fujita, *Acc. Chem. Res.* 42 (2009) 1983-1994.

- [37] A. Inagakia and M. Akita, *Coord. Chem. Rev.* 254 (2010) 1220–1239.
- [38] R. Reithmeier, C. Bruckmeier and B. Rieger, *Catalysts* 2 (2012) 544–571.
- [39] H. Takeda and O. Ishitani, *Coord. Chem. Rev.* 254 (2010) 346–354.
- [40] X. T. Zhou, H. B. Ji and X. J. Huang, *Molecules* 17 (2012) 1149–1158.
- [41] M. E. Ragoussi, J. Malig, G. Katsukis, B. Butz, E. Spiecker, G. Torre de la, T. Torres and D. M. Guldi, *Angew. Chem. Int. Ed.* 51 (2012) 6421–6425.
- [42] K. Kirakci, S. Cordier, C. Perrin, *Z. Anorg. Allg. Chem.* 631 (2005) 411–416.
- [43] H. Schaefer, H. G. Schnering, J. Tillack, F. Kuhn, H. Woehrle, H. Baumann, *Z. Anorg. Allg. Chem.* 353 (1967) 281–310.
- [44] D. Yang, A. Velamakanni, G. Bozoklu, S. Park, M. Stoller, R. Piner, S. Stankovich, I. Jung, D. Field, C. A. Ventrice Jr. and R. S. Ruoff, *Carbon* 47 (2009) 145–152.
- [45] O. Akhavan, *ACS Nano* 4 (2010) 4174–4180.
- [46] S. Ababou-Girard, S. Cordier, B. Fabre, Y. Molard and C. Perrin, *ChemPhysChem* 8 (2007) 2086–2090.
- [47] T. Aubert, F. Cabello-Hurtado, M.-A. Esnault, C. Neaime, D. Lebreton-Chauvel, S. Jeanne, P. Pellen, C. Roiland, L. Le Polles, N. Saito, K. Kimoto, H. Haneda, N. Ohashi, F. Grasset, and S. Cordier, *J. Phys. Chem. C* 117 (2013) 20154–20163.
- [48] T. Aubert, A. Burel, M.-A. Esnault, S. Cordier, F. Grasset, and F. Cabello-Hurtado, *J. Hazard. Mater.* 219 (2012) 111–118.
- [49] O. A. Efremova, M. A. Shestopalov, N. A. Chirtsova, A. I. Smolentsev, Y. V. Mironov, N. Kitamura, K. A. Brylev and A. J. Sutherland, *Dalton Trans.* 43 (2014) 6021–6025.
- [50] H. C. Hsu, I. Shown, H. Y. Wei, Y. C. Chang, H. Y. Du, Y. G. Lin, C. A. Tseng, C. H. Wang, L. C. Chen, Y. C. Lin, and K. H. Chen, *Nanoscale* 5 (2013) 262–268.
- [51] K. P. Loh, Q. Bao, G. Eda, and M. Chhowalla, *Nature Chem.* 2 (2010) 1015–1024.
- [52] F. Bonaccorso, Z. Sun, T. Hasan and A. C. Ferrari, *Nature Photon.* 4 (2010) 611–622.
- [53] G. Eda, C. Mattevi, H. Yamaguchi, H. Kim, and M. Chhowalla, *J. Phys. Chem. C* 113 (2009) 15768–15771.

- [54] P. Kumar, A. Kumar, B. Sreedhar, B. Sain, S. S. Ray, and S. L. Jain, *Chem. Eur. J.* 20 (2014) 6154-6161.
- [55] P. Kumar, A. Bansawal, A. Bansawal, N. Labhsetwar and S. L. Jain, *Green Chem.* 17 (2015) 1605-1609.
- [56] P. Kumar, B. Sain and S. L. Jain, *J. Mater. Chem. A* 2 (2014) 11246-11253.
- [57] G. hee Moon, Y. Park, W. Kim, W. Choi, *Carbon* 49 (2011) 3454-3462.
- [58] Y. T. Liang, B. K. Vijayan, K. A. Gray and M. C. Hersam, *Nano Lett.* 11 (2011) 2865–2870.
- [59] G. Jiang, Z. Lin, C. Chen, L. Zhu, Q. Chang, N. Wang, W. Wei, H. Tang, *Carbon* 49 (2011) 2693-2701.